12th International Symposium on Turbulence and Shear Flow Phenomena (TSFP12)
Osaka, Japan (Online), July 19-22, 2022

LEAN, HIGH EGR RATE TRF-AIR TURBULENT COMBUSTION WITH TUMBLE FLOW IN A CONSTANT VOLUME VESSEL AT ELEVATED PRESSURE

Ryoichi Urasaki
Department of Mechanical Engineering
Tokyo Institute of technology
2-12-1 Ookayama, Meguro-ku, Tokyo, Japan
urasaki.r.aa@m.titech.ac.jp

Yuki Minamoto
Department of Mechanical Engineering
Tokyo Institute of technology
2-12-1 Ookayama, Meguro-ku, Tokyo, Japan
minamoto.y.aa@m.titech.ac.jp

Masayasu Shimura
Department of Mechanical Engineering
Tokyo Institute of technology
2-12-1 Ookayama, Meguro-ku, Tokyo, Japan
shimura.m.aa@m.titech.ac.jp

Mamoru Tanahashi
Department of Mechanical Engineering
Tokyo Institute of technology
2-12-1 Ookayama, Meguro-ku, Tokyo, Japan
tanahashi.m.aa@m.titech.ac.jp

ABSTRACT

To investigate the flame characteristics and flame-wall interaction (FWI) in lean burn spark ignition engine relevant combustion, a direct numerical simulation (DNS) of forced ignition has been performed in a constant volume vessel with a tumble flow. A lean toluene reference fuel (TRF)-air mixture is ignited at the elevated pressure. During the combustion process, a ring-like eddy is generated around the unburnt mixture island which is separated from the main reaction zone. It is shown that the baroclinic torque contributes to the enstrophy production around the unburnt mixture island. In the near-wall region, the low-temperature oxidation reaction becames dominant, and the CO concentration shows a relatively high value even after the flame quenching. In the present study, some statistical properties related to the FWI is also investigated.

INTRODUCTION

Due to the environmental regulations for various combustion devices, high efficiency internal combustion engines are required. To realize highly efficient spark ignition (SI) engines, establishment of combustion technology for lean, high exhaust gas recirculation (EGR) rate, and high compression ratio is required. Under these conditions, decrease of flame propagation speed is a problem. It is considered that the flame speed can be increased by using a high intensity turbulence. However, under such combustion conditions, there are several issues such as ignition difficulty and flame extinction. In addition, high efficient SI engines tend to be smaller. This trend leads the increasing the surface to volume ratio of the engine, and the effect of flame-wall interaction on engine efficiency and emissions will become more significant. However, the characteristics of flame behavior in near wall region under highly efficient SI engines combustion conditions have not been fully understood. Therefore, flame propagation and flame-wall interaction are addressed in the present study considering the spark ignition engines conditions.

In a previous study (Saito *et al.*, 2018), the ignition and flame propagation characteristics of methane and n-heptane air mixtures under IC engine-relevant combustion condition were investigated. However, the unburnt species residue also need to be addressed since since flame-wall interaction can cause wall heat loss, and this effect on overall engine efficiency increases with leaner, diluted and high pressure thermochemical conditions. Also, Yenerdag *et al.* (2016) have been examined fundamental insights into turbulence-flame interactions and heat loss characteristics of hydrogen-air mixture under a elevated pressure condition. However, hydrogen and hydrocarbon fuel yield different combustion characteristics.

Therefore, in this study, a three-dimensional DNS of ignition in a turbulence with a tumble flow has been perfromed considering TRF-air combustion with more than 100 species and 400 elemetary reactions for a high EGR rate and lean premixed mixture in a constant volume vessel at elevated pressure. The DNS results are analysed to clarify the transition mechanism from ignition to flame propagation, flame propagation and flame-wall interaction.

DIRECT NUMERICAL SIMULATIONS

The DNS code used in this study is called Tokyo Tech Combustion Simulation (TTX) that has been developed in previous studies (Tanahashi *et al.*, 2000; Minamoto *et al.*, 2011). A fully-compressible combustion DNS with temperature dependence of transport and thermal properties is performed in a three-dimensional domain in an isochoric condition. The governing equations are for conservation of mass, momentum, energy and species. These equations are discretized using a fourth order central finite difference scheme. The third order explicit Runge-Kutta scheme is used for the time integration. A reduced mechanism for TRF-air combustion (111 species and 416 reactions) (Ogura *et al.*, 2007) is used. The multi-timescale (MTS) method (Gou *et al.*, 2010) is applied for integration of reaction source terms and the correlated dynamic adaptive chemistry and transport (CO-DACT) method (Sun & Ju, 2017) is applied for the chemical and transport properties

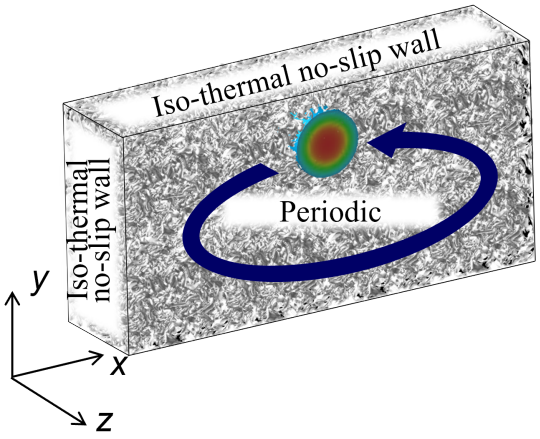

Figure 1. Schematic of the computational domain.

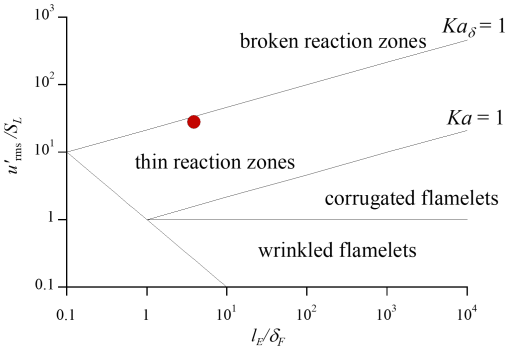

Figure 2. Turbulent combustion conditions of the present DNS (red circle).

for further reduction of computational cost. In the present DNS, iso-thermal no-slip wall condition formulated based on NSCBC (Poinsot & Lelef, 1992; Baum *et al.*, 1995) is applied on the wall surfaces in the x and y directions and periodic boundary condition in the z direction.

Figure 1 shows a schematic of the computational domain. The dimensions of computational domain is $L_x \times L_y \times L_z = 4.8 \times 2.4 \times 1.2$ mm^3, which are discretized by the uniform mesh of $N_x \times N_y \times N_z = 1152 \times 575 \times 288$.

Initially, the vessel is filled with a fully premixed unburnt TRF-air mixture at a uniform preheated temperature of 700 K. The TRF-air mixture is diluted with an exhaust gas consisting of O_2, N_2, H_2O and CO_2 from burnt gas, and the EGR rate is defined as the mass ratio of burnt gas to the mass of unburnt gas. Equivalence ratio of the mixture is set to be 0.6, the EGR rate is set to be 20 %, the initial pressure is set to be 5 atm and the wall temperature is set to 700 K.

Under these thermochemical conditions, the laminar flame speed S_L is 0.277 m/s, the diffusive thickness δ_F is 46.3 μm, the laminar flame thermal thickness $\delta_L = (T_b - T_u)/|\nabla T|_{\max}$ is 0.201 mm. Here, T_b and T_u are the temperature of burnt and unburnt gas mixture in a corresponding one-dimensional laminar flame, respectively. The ignition source is given by placing the one-dimensional laminar flame in a cylindrical shape around the ignition region and kept in the computation to mimic a relatively long-time spark duration in real engines. Considering energy input by spark plug discharge, the temperature at this ignition kernel is fixed to 2000 K. Here, the position of the ignition region is set to the center in the x direction, and the distance from the top wall is set to 0.6 mm in the y direction. The ignition region spans in the z direction. Also, to simulate the tumble flow, the initial mean velocity is set as follows:

$$\Psi = \frac{u_0}{4}\sqrt{L_x L_y}\exp\left[\frac{1}{2}\left(1 - \frac{x^2+y^2}{L_x L_y/16}\right)\right] \tag{1}$$

$$u_{\text{targ}} = \left(\frac{\partial \Psi}{\partial y}, -\frac{\partial \Psi}{\partial x}\right) \tag{2}$$

where, Ψ is the stream function assuming tumble flow, u_{targ} is the initial mainstream velocity and u_0 is the maximum initial mainstream velocity. The initial velocity field is given by overlaying the velocity fluctuation obtained from DNS of homogeneous isotropic turbulence on the initial mean velocity. Figure 2 shows turbulent combustion condition of the present study on the combustion regime diagram (Peters, 1999). The turbulence intensity is set to 28.0 times the unstrained laminar flame speed S_L and the integral length scale l_E is set to 38.7 times the diffusive thickness δ_F. These turbulent combustion conditions is classified in the thin reaction zones regimes as shown in Fig. 2.

LOCAL MIXTURE ISLAND AND BAROCLINIC TORQUE

The temporal evolution of the maximum pressure in the constant volume vessel is shown in Fig. 3. The maximum pressure increases with the spatial development of the turbulent flame. The maximum pressure rises to approximately 1.3 MPa. Figure 4 shows flame structures indicated by iso-surfaces of temperature at 1600K. As shown in Fig. 4, the mixture ignites at the high temperature region and the reaction zone is advected by the tumble flow at the same time as the flame propagates. In the early stage of the flame propagation process, the flame propagates in a direction different from that of the tumble flow. Under the conditions that expected for lean and high-EGR SI engine, unburnt mixture islands are expected to be generated in the transition process from ignition to flame propagation due to the influence of turbulence relatively intense compared to flame scales. In Fig. 4, from 986 to 1116 μs, such an unburnt mixture island exists and its size becomes smaller as the combustion progresses. Also, at the end of the reaction, the flame front approaches to the four walls.

Figure 5 shows iso-surfaces of temperature at 1600 K and the second invariant of gradient of velocity tensor at 10 % of its maximum value at t = 1116 μs. Here, the second invariant in a incompressible limit is used for the visualization of eddies. At this time, more than 70 % of the fuel (in mass) is consumed and mean pressure is elevated to approximately 10 atm. The unburnt mixture remains only in the near wall region expect for the unburnt mixture island which is an interesting flame feature in the present study and denoted as A in Fig. 5.

Here, the eddy structure around the unburnt mixture island is discussed. As shown in Fig. 5, a ring-like eddy (i.e. genus 1 closed surface) appears around the unburnt mixture island. Although this island is created by the separation of the main flame which is sustained by continuous energy input, the ring-like eddy is not observed in the early stage.

Figure 6 shows distributions of velocity fluctuation vector

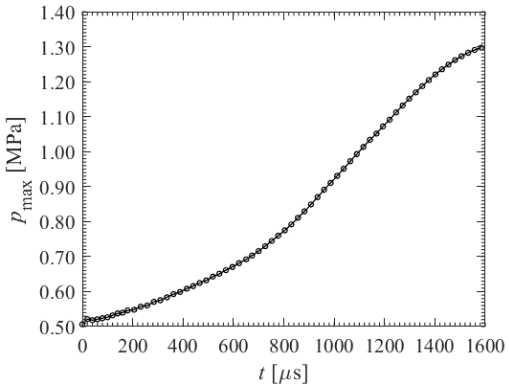

Figure 3. Temporal development of the maximum pressure in the constant volume vessel.

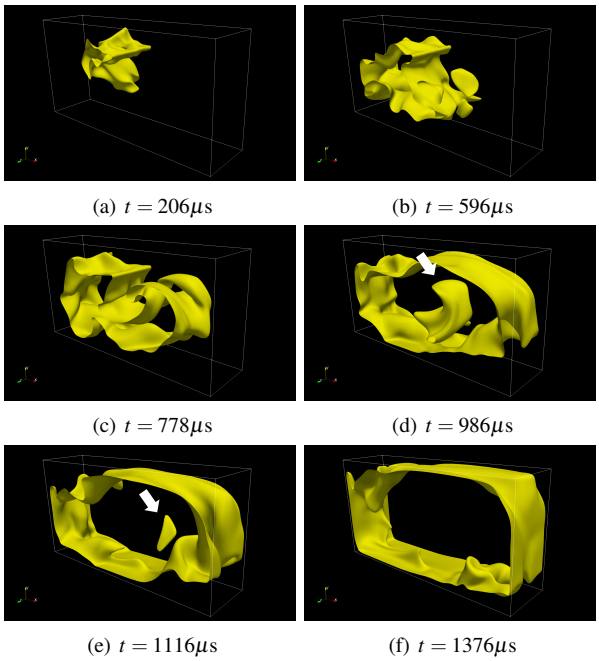

Figure 4. Temporal developments of iso-surfaces of temperature at 1600 K at (a)$t = 206$ μs, (b)$t = 596$ μs, (c)$t = 778$ μs, (d)$t = 986$ μs, (e)$t = 1116$ μs, (f)$t = 1376$ μs. Arrows indicate the unburnt mixture island.

and temperature, heat release rate, mass fraction of CH_2O and fuel around the unburnt mixture island (show in Fig. 5) on a $x-y$ plane (z = 0.0 mm) at 1116 μs. Here, heat release rate shows a high value around the unburnt mixture island, where the fuel species still exist. Also, the temperature at the unburnt mixture island is approximately 1300 K which is higher than the initial temperature of 700 K and the CH_2O is produced. From the velocity fluctuation vector, it can be seen that a ring-like eddy is generated around this unburnt mixture island.

Since there may be a link between the creation of such an unburnt mixture island and the ring-like eddy, the enstrophy transport equation is analyzed to investigate the origin of the ring-like eddy. The enstrophy transport equation can be written as:

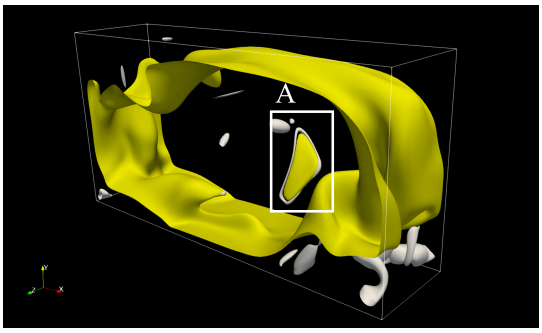

Figure 5. Iso-surfaces of temperature at 1600K and the second invariant of gradient of velocity tensor (in the incompressibility limit) at 10 % of its maximum value at $t = 1116$ μs.

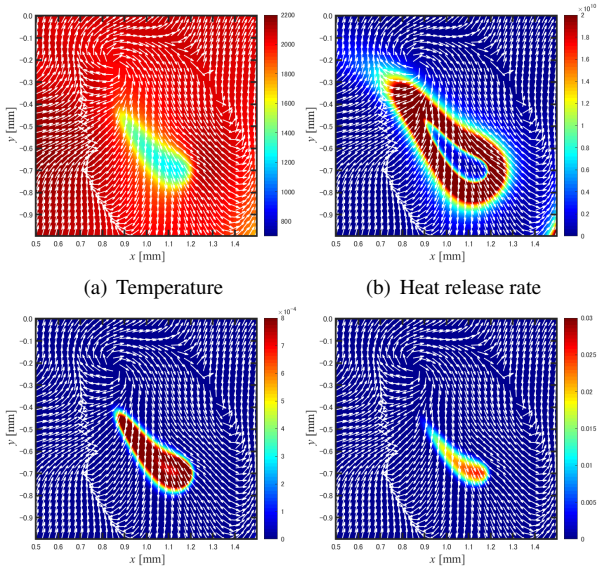

Figure 6. Distributions of velocity fluctuation vector and (a)temperature, (b)heat release rate, (c)mass fraction of CH_2O and (d)fuel (show in Fig.5) on a $x-y$ plane (z = 0.0 mm) around the unburnt mixture island at 1116 μs.

$$\frac{D\omega^2}{Dt} = \omega\cdot(\omega\cdot\nabla)\boldsymbol{u} + \omega\cdot\nu\Delta\omega - \omega^2(\nabla\cdot\boldsymbol{u}) + \omega\cdot\frac{1}{\rho^2}\nabla\rho\times\nabla P, \tag{3}$$

where ω and ν indicate vorticity and kinetic viscosity respectively. Figure 7 shows distribution of the baroclinic torque term on a $x-y$ plane around region A shown in Fig.5. Intense baroclinic torque exists around the unburnt mixture island, and the baroclinic torque contributes to both destruction and production of enstrophy in this region. Figure 8 shows the conditional average of the enstrophy transport terms conditioned based on the reaction progress variable. The samples collected around the unburnt mixture island, and reaction progress variable is based on the temperature. On an average sense, the baroclinic torque contributes to the enstrophy destruction while both destruction and production exist locally as shown in Fig. 7.

Therefore, the evolution of the ring-like eddy tends to be dissipative, although it yields some local fluctuations. The existence of this destruction and production mechanisms of the

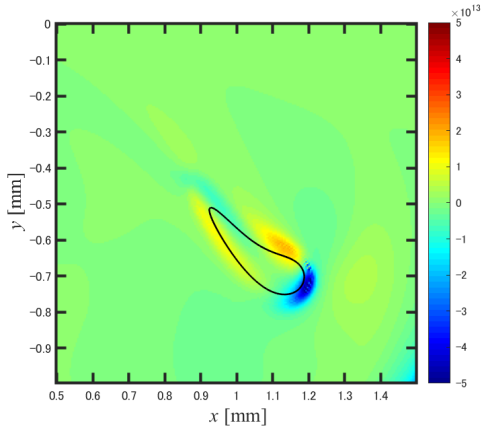

Figure 7. Distributions of baroclinic torque on a $x-y$ plane (z = 0.0 mm) around the unburnt mixture island at 1116 μs. Contour line corresponds to the unburnt mixture island.

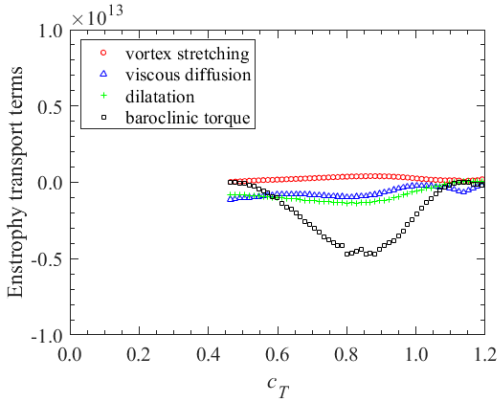

Figure 8. Enstrophy transport budget conditioned with the progress variable based on temperature in the unburnt mixture island.

ring-like eddy suggests that the eddy may enhance the scalar mixing between hot and fresh mixtures near the unburnt mixture island to promote combustion processes.

NEAR-WALL FLAME BEHAVIOR

To realize high efficiency and low emission engines, near-wall behaviors of lean and diluted flame are important. Figure 9 shows near-wall distributions of heat release rate and mass fraction of fuel species, CO and $C_7H_{14}OOH$ on a typical $x-y$ plane. Here, the flame-wall interaction region is enlarged. The right side of the shown region corresponds to downstream of the tumble flow.

As shown in Figs. 9(a) and (b), small heat release rate value is observed in the downstream region ($x > -0.2$ mm), and this is because the fuel is already consumed almost completely. In the downstream region, the CO concentration shows a moderate value, and the CO consumption process is believed to yield a relatively large timescale in this region. In the upstream region ($x < -0.4$ mm), concentration of $C_7H_{14}OOH$, which is an indicator of the low-temperature oxidation reaction, shows a relatively high value in the near-wall region and CO concentration is high between the wall and high heat release rate region.

In the present study, statistical properties related to the FWI is also investigated. The local flame front is identified

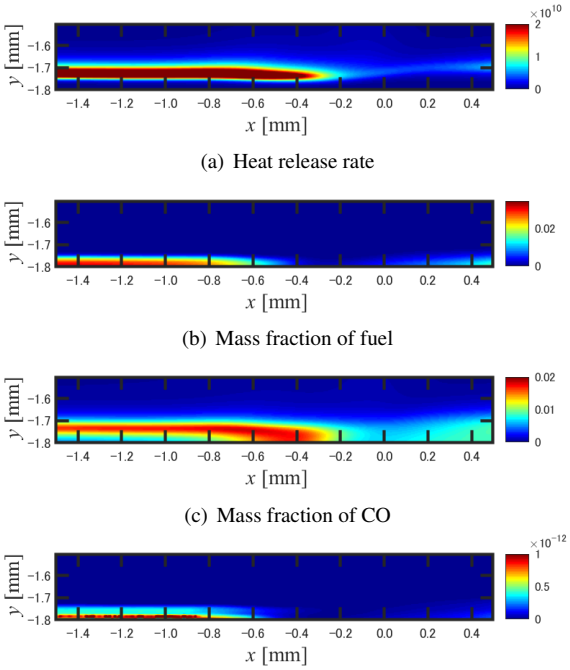

(a) Heat release rate

(b) Mass fraction of fuel

(c) Mass fraction of CO

(d) Mass fraction of $C_7H_{14}OOH$

Figure 9. Distributions of (a)heat release rate, mass fraction of (b)fuel, (c)CO, (d)$C_7H_{14}OOH$ on a $x-y$ plane (z = 0.55 mm) at 1324 μs.

only when there is a local maximum exist in the heat release rate distribution in the region within the laminar flame thermal thickness δ_L from the wall surface. The distance between the flame front and the wall defined by the maximum heat release rate is defined as d_w, which is the flame-wall distance.

Figure 10 shows the conditional average of the maximum heat release rate ΔH_{max} that is used in the identification of the flame front, conditioned based on d_w. The conditional average was also conditioned based on the mean pressure in the domain, $0.9 < \langle p \rangle < 1.0$, $1.0 < \langle p \rangle < 1.1$, $1.1 < \langle p \rangle < 1.2$, and $1.2 < \langle p \rangle$ (MPa). When d_w is large, $\log_{10}(\Delta H_{max})$ deviates approximately 0.3 for different $\langle p \rangle$, while the deviation increases to be approximately 0.8 at flame quenching distance (e.g. $d_w \approx 35$ μm).

Figure 11 shows the conditional average of the wall heat flux Φ conditioned based on the flame distance d_w from the wall and the mean pressure of the vessel $\langle p \rangle$. The heat loss through the wall increases with the decrease of the flame distance from the wall, and this trend is independent on $\langle p \rangle$.

When the flame-wall distance becomes smaller than 100 μm, the wall heat flux increases rapidly, and the maximum heat flux exceeds 1.8 MW/m^2. The minimum flame-wall distance is about 50 μm and this distance is also independent on the pressure. It is interesting that for the $1.2 < \langle p \rangle$ samples the maximum heat flux tends to decrease near the wall, while for the other samples the heat flux monotonically increases with the decrease of d_w. This non-monotonic behaviour of Φ for the $1.2 < \langle p \rangle$ samples is still unclear.

Figure 12 shows the conditional average of the mean value of $\langle \rho Y_{CO} \rangle$ conditioned based on the flame distance from the wall. Here, $\langle \rho Y_{CO} \rangle$ is obtained by averaging ρY_{CO} over the distance between the wall and the identified flame front location.

Figure 12 shows that the CO concentration near the wall increases as the flame approaches the wall until $d_w \approx 50$ μm. However, for $d_w < 50$ μm, the CO concentration decreases.

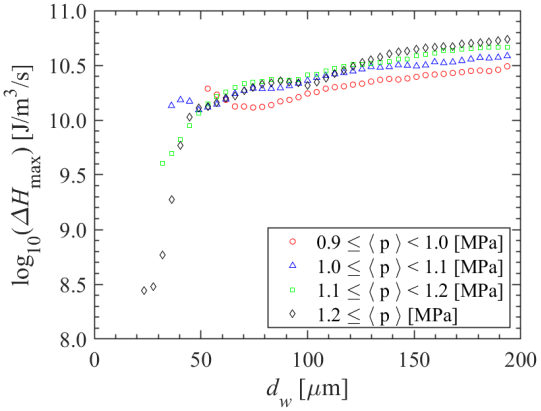

Figure 10. The conditional average of the maximum heat release rate that is used in the identification of the flame front based on the flame distance from the wall.

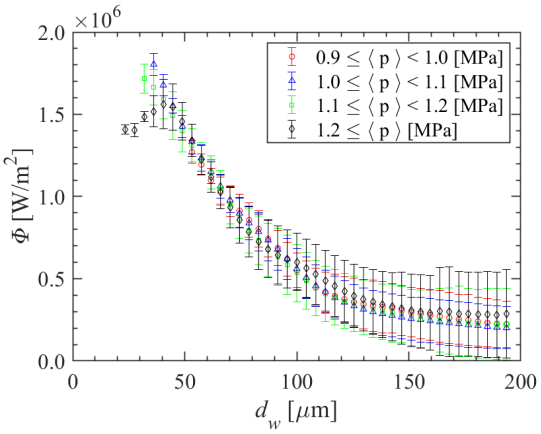

Figure 11. The conditional average of the wall heat flux conditioned based on the flame distance from the wall.

Figure 13 shows the conditional average of the convection (C), diffusion (D) and reaction (R) terms in the CO transport equation conditioned based on d_w. The samples are taken from the second mesh point inside the wall. Figure 13 shows that diffusion term dominate to the transport of CO near the wall compared with other terms. The large CO concentration in the region of $d_w > 50$ μm in Fig. 12 is due to the diffusion contribution. However, for $d_w < 50$ μm, the diffusion term yields negative values, indicating that CO is transported away from the wall by diffusion.

CONCLUSIONS

A direct numerical simulation (DNS) of forced ignition in a constant volume vessel with a tumble flow has been performed for a lean TRF-air mixture at high EGR rate at elevated pressure. During the combustion process, a ring-like eddy is generated around the unburnt mixture island which is separated from the main flame. It is shown that the baroclinic torque term contributes to the enstrophy production and destruction around the unburnt mixture island.

In the near wall region, the low-temperature oxidation reaction is increased, and the CO concentration shows a relatively high value even after the flame quenching. The wall heat flux increases with the decrease of the flame distance from the wall, which is independent on the averaged pressure for low pressure samples. For the high pressure samples, the wall heat

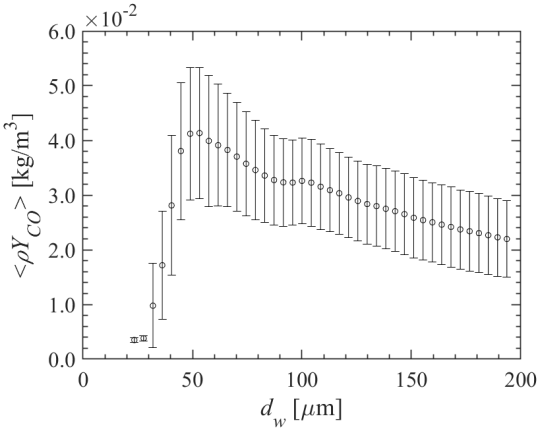

Figure 12. The conditional average of the mean value of $\langle \rho Y_{CO} \rangle$ conditioned based on the flame distance from the wall.

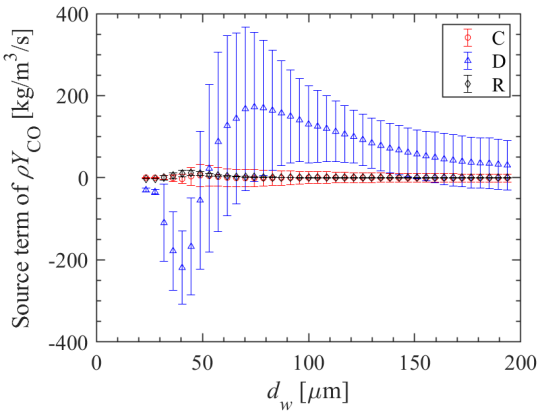

Figure 13. The conditional average of the convection (C), diffusion (D) and reaction (R) terms in the CO transport equation on the wall conditioned based on the flame distance from the wall.

flux tends to decrease near the wall, but this mechanism is still unclear. The concentration of CO in near-wall region is dominated by the diffusion process.

ACKNOWLEDGEMENTS

This study is the result of a collaborative research program with the Research association of Automotive Internal Combustion Engines (AICE) for fiscal year 2020 and 2021.

REFERENCES

Baum, M., Poinsot, T. & Thevenin, D. 1995 Accurate boundary conditions for multicomponent reactive flows. *Journal of Computational Physics* **116**, 247–261.

Gou, X., Sun, W., Chen, Z. & Ju, Y. 2010 A dynamic multi-timescale method for combustion modeling with detailed and reduced chemical kinetic mechanisms. *Combustion and Flame* **157**, 1111–1121.

Minamoto, Y., Fukushima, N., Tanahashi, M., Miyauchi, T., Dunstan, T. & Swaminathan, N. 2011 Effect of flow-geometry on turbulence-scalar interaction in premixed flames. *Physics of Fluids* **23**, 125107.

Ogura, T., Sakai, Y., Miyoshi, A., Koshi, M. & Degaut, P. 2007 Modeling of the oxidation of primary reference fuel in the

presence of oxygenated octane improvers: Ethyl tert-butyl ether and ethanol. *Energy & Fuels* **21**, 3233–3239.

Peters, N. 1999 The turbulent burning velocity for large-scale and small-scale turbulence. *Journal of Fluid Mechanics* **384**, 107–132.

Poinsot, T. & Lelef, S. 1992 Boundary conditions for direct simulations of compressible viscous flows. *Journal of Computational Physics* **101**, 104–129.

Saito, N., Minamoto, Y., Yenerdag, B., Shimura, M. & Tanahashi, M. 2018 Effects of turbulence on ignition of methane–air and n-heptane–air fully premixed mixtures. *Combustion Science and Technology* **190**, 451–469.

Sun, W. & Ju, Y. 2017 A multi-timescale and correlated dynamic adaptive chemistry and transport (co-dact) method for computationally efficient modeling of jet fuel combustion with detailed chemistry and transport. *Combustion and Flame* **184**, 297–311.

Tanahashi, M., Fujimura, M. & Miyauchi, T. 2000 Coherent fine-scale eddies in turbulent premixed flames. *Proceedings of the Combustion Institute* **28**, 529–535.

Yenerdag, B., Minamoto, Y., Naka, M. & Tanahashi, M. 2016 Flame propagation and heat transfer characteristics of a hydrogen-air premixed flame in a constant volume vessel. *International Journal of Hydrogen Energy* **41**, 9679–9689.